Parkinsonism and Related Disorders 81 (2020) 96–102

Contents lists available at ScienceDirect

Parkinsonism and Related Disorders

journal homepage: www.elsevier.com/locate/parkreldis

Patterns of diffusion kurtosis changes in Parkinson's disease subtypes

Alzbeta Sejnoha Minsterova [a,b], Patricia Klobusiakova [a,b], Adrian Pies [a,b], Zoltan Galaz [c], Jiri Mekyska [c], Lubomira Novakova [a], Nela Nemcova Elfmarkova [a], Irena Rektorova [a,d,*]

[a] Applied Neuroscience Research Group, Central European Institute of Technology – CEITEC, Masaryk University, Brno, Czech Republic
[b] Faculty of Medicine, Masaryk University, Brno, Czech Republic
[c] Department of Telecommunications, Brno University of Technology, Brno, Czech Republic
[d] First Department of Neurology, Faculty of Medicine and St. Anne's University Hospital, Masaryk University, Brno, Czech Republic

ARTICLE INFO

Keywords:
MRI
Diffusion kurtosis imaging
Parkinson's disease
Mild cognitive impairment
Diagnostic marker

ABSTRACT

Background: Diffusion kurtosis imaging has been applied to evaluate white matter and basal ganglia microstructure in mixed Parkinson's disease (PD) groups with inconclusive results.
Objectives: To evaluate specific patterns of kurtosis changes in PD and to assess the utility of diffusion imaging in differentiating between healthy subjects and cognitively normal PD, and between PD with and without mild cognitive impairment.
Methods: Diffusion scans were obtained in 92 participants using 3T MRI. Differences in white matter were tested by tract-based spatial statistics. Gray matter was evaluated in basal ganglia, thalamus, hippocampus, and motor and premotor cortices. Brain atrophy was also assessed. Multivariate logistic regression was used to identify a combination of diffusion parameters with the highest discrimination power between groups.
Results: Diffusion kurtosis metrics showed a significant increase in substantia nigra ($p = 0.037$, Hedges' $g = 0.89$), premotor ($p = 0.009$, Hedges' $g = 0.85$) and motor ($p = 0.033$, Hedges' $g = 0.87$) cortices in PD with normal cognition compared to healthy participants. Combined diffusion markers in gray matter reached 81% accuracy in differentiating between both groups. Significant white matter microstructural changes, and kurtosis decreases in the cortex were present in cognitively impaired versus cognitively normal PD. Diffusion parameters from white and gray matter differentiated between both PD phenotypes with 78% accuracy.
Conclusions: Increased kurtosis in gray matter structures in cognitively normal PD reflects increased hindrance to water diffusion caused probably by alpha-synuclein-related microstructural changes. In cognitively impaired PD, the changes are mostly driven by decreased white matter integrity. Our results support the utility of diffusion kurtosis imaging for PD diagnostics.

1. Introduction

Parkinson's disease (PD) is a synucleinopathy characterized by misfolded alpha-synuclein accumulation in Lewy bodies and Lewy neurites, alpha-synuclein-related activation of microglia and neuroinflammation, and brain degeneration reflected by gross brain atrophy [1–3], although other comorbid brain pathologies such as vascular changes or Alzheimer's disease-related pathology may also co-occur [1]. Both animal and human studies [4–6] have suggested that diffusion tensor imaging (DTI), and particularly diffusion kurtosis imaging (DKI), may well serve as early biomarkers of white matter (WM) and gray matter (GM) microstructural brain changes in PD. Increased kurtosis is an indicator of the heterogeneous environment with restrictions to diffusion. The mean kurtosis (MK) is a measure of diffusion kurtosis in the voxel. The axial kurtosis (AK) is the kurtosis along the direction of axons, and radial kurtosis (RK) describes kurtosis in a perpendicular direction. A recent review and meta-analysis of the results of conventional DTI findings in PD [7] reported specific changes in fractional anisotropy (FA) and/or mean diffusivity (MD), particularly within the substantia nigra (SN), the corpus callosum, and the cingulate and temporal cortices, as well as in the corticospinal tract.

A clear limitation of a DTI model is the oversimplified assumption that the probability of water diffusion follows the Gaussian distribution. The complexity of the brain tissue leads to serious alterations from this pattern, which is particularly relevant to GM [4,8,9]. Unlike conventional DTI, DKI allows for quantification of the non-Gaussian diffusion as

* Corresponding author. Applied Neuroscience Research Group, Central European Institute of Technology – CEITEC, Masaryk University, Brno, Czech Republic.
E-mail address: irena.rektorova@ceitec.muni.cz (I. Rektorova).

https://doi.org/10.1016/j.parkreldis.2020.10.032
Received 23 July 2020; Received in revised form 15 October 2020; Accepted 17 October 2020
Available online 20 October 2020

it uses multi-shell acquisition [8]. Therefore, DKI may provide more precise information about the microstructural properties and both GM and WM tissue heterogeneity [4,8,9]. Having said that, only few studies have used DKI to assess WM and subcortical GM changes in PD as compared to healthy controls (HC) so far with inconsistent results [6,10,11]. The inconsistency in the direction of DKI parameters changes may stem from the small sample sizes and from the fact that the recruited subjects were not cognitively examined in detail, and thus may have represented heterogeneous groups of PD subjects with normal cognition (PD-NC) and with MCI (PD-MCI). Another potential source of inconsistent results may arise from different statistical approaches employed, since the diffusion MRI is lacking a golden standard for the data analysis [12].

Therefore, in our cross-sectional study we focused on the evaluation of microstructural changes in PD with various clinical subtypes (PD-NC, PD-MCI) as compared to HC. Having been motivated by our translational DKI research in animal models of PD [4,13,14] we used the DKI parameters to measure changes particularly in GM within the basal ganglia, hippocampus and motor (M1)/premotor (PMC) cortical areas, i.e. the cortical output areas of the motor striato-thalamo-cortical loop [15]. Diffusion changes in the WM skeleton were also assessed. In order to keep the results comparable with previous DTI studies, we additionally used the conventional DTI approach with single-shell acquisition.

The main goal was to describe specific patterns of DKI/DTI changes in PD-NC and to evaluate whether DKI can serve as a diagnostic biomarker of this PD phenotype. We hypothesized that we would be able to identify specific patterns of DKI changes particularly in our subcortical and cortical GM regions of interest (ROIs). The secondary objective was to describe microstructural correlates of MCI in PD and evaluate how accurately diffusion MRI can identify the PD-MCI subtype in the PD population. This is clinically relevant since MCI in PD is a clear risk factor for PD-dementia and a more malignant disease course [1,16]. In line with the literature, we suspected decreased integrity of WM along with distinct cortical brain atrophy in PD-MCI [2,7].

2. Patients and methods

2.1. Subjects in the cohort

We analyzed DKI, DTI, and structural MRI data of PD patients and HC from a previously published cohort [17–19]. In brief, PD patients were recruited based on criteria of established PD-MCI [16] and PD [20]. All subjects underwent cognitive testing covering all cognitive domains and an MRI examination (for details see below). Exclusion study criteria included alcohol/drug abuse, hallucinations or visual misperceptions, and any diagnosed psychiatric disorder. None of the patients was taking any psychoactive drugs. Each subject signed an informed consent form and the study was approved by the local ethics committee.

2.2. Neuropsychological assessment

A cognitive test battery described in our previous publications [18,19] was used. For a description of the cognitive test battery, see Supplementary Materials. The cognitive domain Z-scores were computed as the average Z-scores of the tests included in the particular domain [19] and each domain was inspected for cognitive decline. Subjects who scored below −1.5 SD in two tests in at least one cognitive domain but with preserved independence in functional abilities were categorized as PD-MCI.

2.3. MR acquisition

Imaging was performed on a 3T Siemens Prisma scanner (Siemens Corp., Erlangen, Germany) at CEITEC, Masaryk University, Brno, Czech Republic. T1 imaging was performed with MPRAGE sequence with 240 sagittal slices, TR = 2300 ms, TE = 2.36 ms, FOV = 256 mm, FA = 8°, matrix size 256 × 256, voxel size 1 × 1 × 1 mm. DKI sequence with the following parameters was used: 30 non-colinear diffusion directions for each of b-values 500, 1000, 2000, and 4000 s/mm^2 and 10 acquisitions without diffusion weighting (b = 0 s/mm^2), TR = 9300 ms, TE = 97 ms, FOV = 228 mm, acquisition matrix 114 × 114 × 64, voxel size 2 × 2 × 2 mm. Three acquisitions with b = 0 s/mm^2 with opposite phase polarity were acquired. The total acquisition time for the diffusion MRI was 21:31.

2.4. DKI/DTI data preprocessing

FSL software version 5.0.9 was used for the preprocessing. Data were first corrected for susceptibility-induced distortions using the topup tool and for movement and eddy current artifacts using the eddy tool. Non-brain tissue voxels were automatically excluded using the Brain Extraction Toolbox. The output brain masks were checked one by one and corrected manually when needed.

To model the kurtosis tensor in DKI data, the Diffusional Kurtosis Estimator software (https://www.nitrc.org/projects/dke) implemented in MATLAB (The MathWorks, Inc.) was used. The robust fitting option using the robust estimation of tensor by outlier rejection algorithm was used. Parameters of interest were fractional anisotropy (DKI_FA), MK, RK, and AK.

The DTI dataset contained single-shell data (b = 1000 s/mm^2). FSL function DTIFIT was used to model the diffusion tensor of each voxel in the DTI data and parametric maps were calculated. Parameters of interest were DTI_FA, MD, radial diffusivity (RD), and axial diffusivity (AD).

2.5. DKI/DTI data analysis in our subcortical and cortical GM ROIs

Masks of our subcortical ROIs, i.e. bilateral: putamen, caudate nucleus, globus pallidus and thalamus, and of the hippocampus were calculated using T1-weighted images in FreeSurfer 6.0 (http://surfer.nmr.mgh.harvard.edu). The mean SN mask was also created, for details see Supplementary Materials and Figure S1. The mask of cortical GM was obtained using the SPM12 (http://www.fil.ion.ucl.ac.uk/spm/software/spm12) segmentation tool. Masks of the cortical ROIs were obtained from the Juelich histological atlas. For each subject, the mask of cortical GM was multiplied by masks of M1 and PMC. All subjects' resulting masks were visually inspected for segmentation errors and the resulting mask was registered to each subject's native diffusion-weighted space.

To identify differences between group pairs (PD-NC vs. HC, PD-MCI vs. PD-NC, PD-MCI vs. HC), the non-parametric permutation based approach using the permutation analysis of linear model (PALM) tool in FSL and general linear model was used. The number of permutations was set at 5000. Data were controlled for the effects of age, gender, education, and LED (just for the PD groups). The $\alpha = 0.05$ was set as the significance level. Effect sizes (ES) were additionally calculated using the Hedges' g (for details about the formula, see Supplementary Material).

2.6. DKI/DTI data analysis of WM: exploratory analysis using TBSS

After the above-mentioned preprocessing and quality control, the data underwent tract-based spatial statistics (TBSS) analysis [21].

We first performed a voxel-wise nonlinear registration of all subjects' FA maps to the chosen target. The FMRIB58_FA_1 mm image was used as a target. The whole dataset was then affine-transformed to MNI152 standard space with 1x1x1 mm resolution. The FA image was created and the skeleton of WM tracts common for all subjects was calculated at a threshold of 0.2. Individual FA maps of all subjects were projected onto the skeleton. Other parametric maps were handled similarly. They were nonlinearly registered to a common space and then projected onto the FA skeleton.

The voxel-wise statistics across subjects were calculated using the general linear model and non-parametric permutation test by the FSL Randomise tool. The number of permutations was set at 5000 and the threshold-free cluster enhancement method was used. Data were controlled for the effects of age, gender, education, and LED (just for the PD groups). The $\alpha = 0.01$ was set as the significance level. Regions showing significant differences between groups were defined using the JHU ICBM-DTI-81 W M labels atlas and the Juelich histological atlas provided by FSL.

2.7. Deformation-based morphometry

The DBM analysis [22] was conducted using the Computational Anatomy Toolbox (CAT 12, http://dbm.neuro.uni-jena.de/cat/) and SPM12 software running under MATLAB2014b. The Jacobian determinant for each voxel in normalized space was calculated for each subject and the resulting maps were spatially smoothed using the Gaussian filter kernel with a FWHM of 6 mm. Smoothed Jacobian determinant volumes were compared across groups by applying a two-sample *t*-test. Results were controlled for age, gender, education and LED (just for the PD groups). The FDR correction was used and the $p_{FDR} = 0.05$ was set as the significance level.

2.8. Differential analysis

To identify an information-rich, parsimonious combination of parameters with the highest discrimination power between the groups, we employed the multivariate class-weighted logistic regression with L1 regularization (LASSO). The DKI and DTI parameters from all GM ROIs and WM skeleton served as the input features. Before training, all features were standardized on a per feature basis to have zero mean and the standard deviation of one. To get the optimal trade-off between the models' complexity and the ability to generalize, we fine-tuned the models' regularization strength parameter via the grid-search technique over a grid of 100 numbers evenly distributed on a logarithmic scale: <log10(-2)– log10(0.25)>. The grid-search was set-up to use the stratified 5-fold cross-validation with 20 repetitions aiming at optimizing Matthew's correlation coefficient. Finally, we used the Receiver Operator Characteristics (ROC) curve to fine-tune the trained models' decision thresholds to achieve the optimal trade-off between the models' sensitivity and specificity. Using the fine-tuned decision thresholds, we evaluated the models' classification performance using the stratified 5-fold cross-validation. The ROC curves were plotted using the predicted labels' probabilities obtained via the cross-validation procedure employed during the final evaluation of the trained models. Resulting regression coefficients were considered as feature importances. For the analysis, we used the Python programming language (v. 3.7) and the scikit-learn (https://scikit-learn.org/stable/) machine learning library (v. 0.22.2).

3. Results

3.1. Demographic, clinical, and cognitive data

The cohort including HC and PD subjects consisted of 107 participants. Altogether 15 subjects were excluded from the diffusion data analysis: 12 subjects (10 HC, 2 PD-MCI) were excluded because of excessive movement or susceptibility artifacts in the MR data; 3 subjects (1 HC, 2 PD-MCI) did not finish the MR protocol. For detailed demographic and clinical information on the final dataset, which consists of 92 subjects, see Table 1.

There was a significant difference in age and gender distribution between HC and PD groups. No difference was observed in time from diagnosis between the PD-NC and PD-MCI groups. Therefore, our PD groups reflect different PD phenotypes (with and without MCI) rather than different stages of PD progression.

Table 1
Demography and clinical characteristics: all values are depicted as mean ± standard deviation. MMSE – Mini mental state examination; GDS – Geriatric depression scale; UPDRS III - Unified Parkinson's Disease Rating Scale, part III (Motor Examination); LED – Levodopa equivalent dose; H&Y score - Hoehn & Yahr scale; * marks differences that remained significant after FDR correction.

	HC	PD-NC	PD-MCI	PD-NC versus HC (p-value)	PD-MCI versus PD-NC (p-value)	PD-MCI versus HC (p-value)
N	48	23	21	–	–	–
Gender (M/F)	16/32	17/6	16/5	0.001*	0.862	0.001*
Age	66.7 ± 7.5	61.0 ± 8.4	64.8 ± 10.7	0.008	0.145	0.648
Years of education	15.6 ± 2.6	16.2 ± 3.3	14.5 ± 3.0	0.472	0.045	0.046
MMSE	28.5 ± 1.2	28.2 ± 1.2	26.9 ± 2.0	0.234	0.018*	<0.001*
GDS	2.46 ± 2.7	2.82 ± 2.9	2.76 ± 2.2	0.549	0.774	0.357
UPDRS III	–	17.6 ± 8.7	17.5 ± 8.6	–	0.832	–
LED	–	822.5 ± 536.2	861.5 ± 486.2	–	0.655	–
H&Y score	–	1.82 ± 0.46	1.76 ± 0.53	–	0.745	–
Side of symptom onset (L/R/B)	–	13/9/1	6/14/1	–	0.167	–
Years from diagnosis	–	5.0 ± 3.1	5.5 ± 4.5	–	0.981	–
Cognitive domain Z-scores						
Memory	0.59 ± 0.49	0.24 ± 0.74	−0.63 ± 0.73	0.052	0.001*	<0.001*
Attention	−0.04 ± 0.65	−0.27 ± 0.91	−1.15 ± 0.94	0.212	0.004*	<0.001*
Executive	0.52 ± 0.75	0.35 ± 0.67	−0.60 ± 0.91	0.403	<0.001*	<0.001*
Visuospatial	0.41 ± 0.59	0.44 ± 0.55	0.01 ± 0.80	0.614	0.244	0.0826
Language	0.45 ± 0.42	0.31 ± 0.62	0.03 ± 0.82	0.050	0.076	0.0032*

3.2. MRI data results

3.2.1. Evaluation of GM microstructure

Only differences between groups that revealed both statistical significance and large ES (Hedges' $g > 0.8$) or medium ES (Hedges' $g > 0.5$) are described in the text below. For all p-values, ESs and DKI/DTI values, see Supplementary Materials, Table S1 and Table S2.

3.2.1.1. PD-NC versus HC. In PD-NC as compared to HC we found increases of DKI_FA in the SN ($p = 0.037$, Hedges' $g = 0.89$), and AK in M1 and PMC ($p = 0.033$, Hedges' $g = 0.87$ and $p = 0.009$, Hedges' $g = 0.85$, respectively).

3.2.1.2. PD-MCI versus PD-NC. In PD-MCI as compared to PD-NC we found decreases of AK in M1 ($p = 0.01$, Hedges' $g = 0.85$), DKI_FA in thalamus ($p = 0.007$, Hedges' $g = 0.55$), MK in thalamus, M1 and hippocampus ($p = 0.015$, Hedges' $g = 0.50$, $p = 0.013$, Hedges' $g = 0.62$ and $p = 0.011$, Hedges' $g = 0.62$, respectively), RK in thalamus, M1 and hippocampus ($p = 0.006$, Hedges' $g = 0.57$, $p = 0.026$, Hedges' $g = 0.50$ and $p = 0.006$, Hedges' $g = 0.70$, respectively), AK in PMC ($p = 0.034$, Hedges' $g = 0.66$) and DTI_FA in thalamus and hippocampus ($p = 0.002$, Hedges' $g = 0.76$ and $p = 0.018$, Hedges' $g = 0.60$, respectively).

Boxplots for significant differences with large ES (Hedges' $g \geq 0.8$) are shown in Fig. 1. Of note, in the PD-MCI group, the values of DKI parameters of interest were between those in the PD-NC and HC groups;

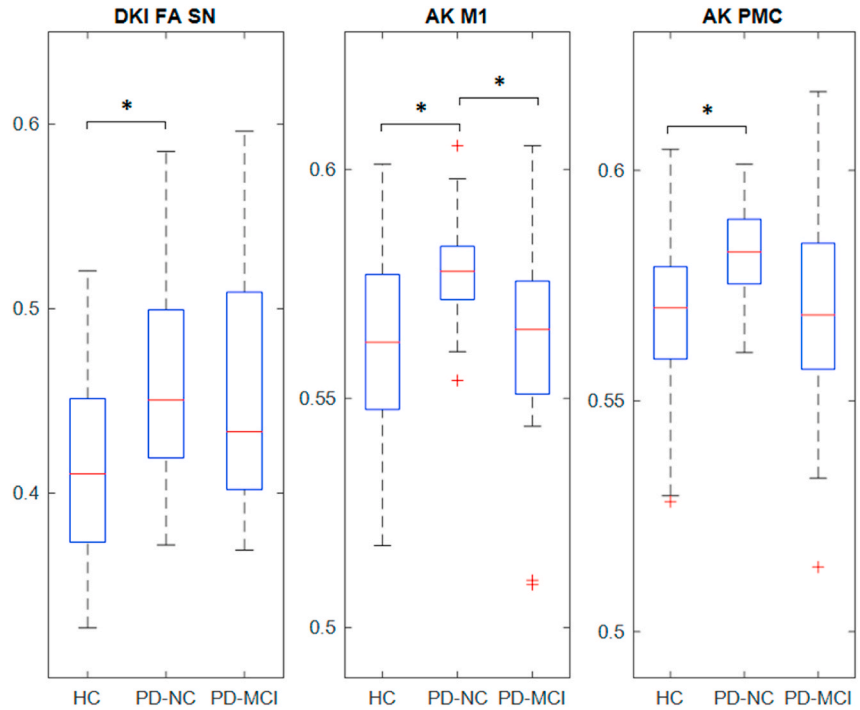

Fig. 1. Visualization of markers in GM; * marks comparisons that revealed both statistical significance and large effect size (Hedges' g > 0.8).

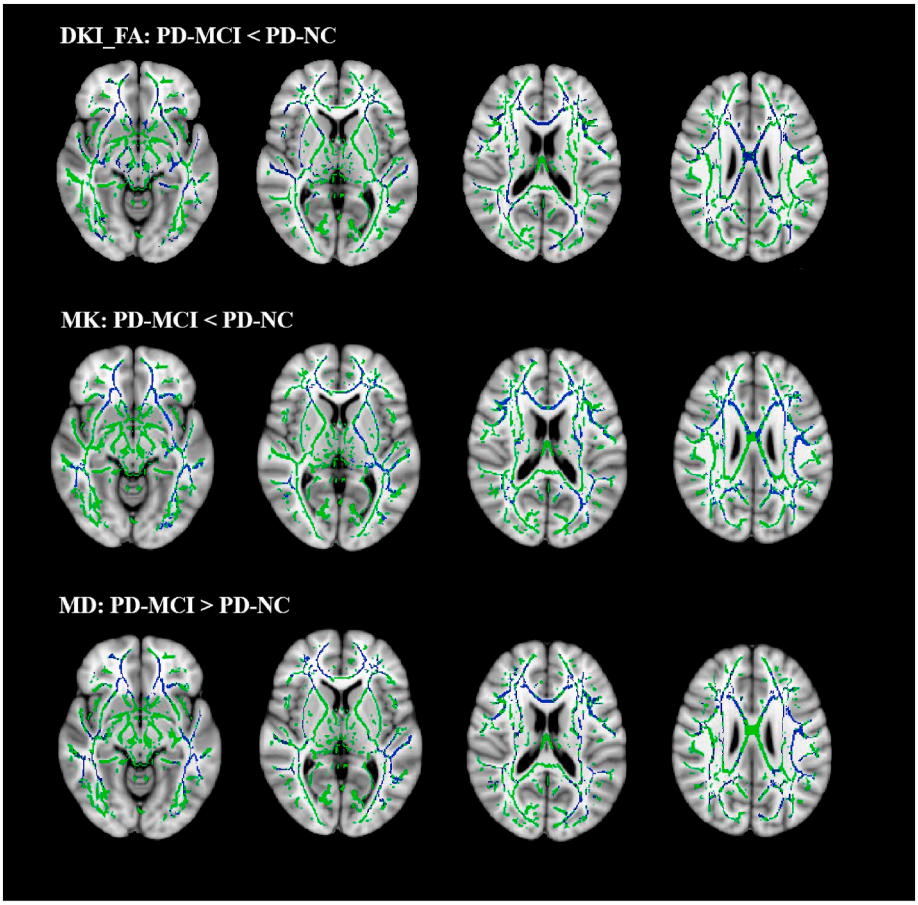

Fig. 2. TBSS results, contrast PD-MCI to PD-NC; blue – significant differences (level of significance 0.01); green – FA skeleton. (For interpretation of the references to colour in this figure legend, the reader is referred to the Web version of this article.)

see Fig. 1 and Supplementary Materials, Table S1.

3.2.1.3. PD-MCI versus HC. No differences in subcortical or cortical structures were detected.

3.2.2. Evaluation of WM microstructure

3.2.2.1. PD-NC versus HC. The TBSS revealed no significant differences between the two groups.

3.2.2.2. PD-MCI versus PD-NC/HC. TBSS revealed widespread DKI/DTI changes in the PD-MCI as compared to the PD-NC (see Fig. 2) and HC groups. See Supplementary Materials for all results.

3.2.3. Evaluation of brain atrophy using deformation-based morphometry

DBM revealed brain atrophy in the PD-MCI as compared to HC in the frontal pole bilaterally ($p_{FDR} = 0.05$), see Figure S2 in Supplementary Materials. No other differences were detected between the groups.

3.3. Differential analysis

We achieved 81% accuracy (ACC), 92% sensitivity (SEN), and 71% specificity (SPE) in discriminating between PD-NC and HC, the following features were selected by the logistic regression (feature importance/weights are in parentheses): L1_thalamus (2.53), DTI_FA_palidum (2.49), DKI_FA_caudate (2.05), DTI_FA_putamen (1.72), AK_PMC (1.66), DTI_FA_caudate (1.49), RK_thalamus (1.26), DKI_FA_putamen (1.20).

For discriminating PD–NC and PD–MCI we achieved 78% ACC, 83% SEN, and 74% SPE. The following features were selected by the logistic regression: MK_WM (0.43), DTI_FA_WM (0.33), AK_M1 (0.05). For ROC curves, see Fig. 3

4. Discussion

The PD pathology is complex and affects the brain tissue structure by various processes that are difficult to separate with MRI methods. In early PD, these include particularly alpha-synuclein accumulation [3], microglial activation [23], and axonal sprouting [24], all of which are processes that increase the restrictions to the diffusion in the environment. On the other hand, a more malignant course of the disease linked with early cognitive impairment is characterized by major neurodegeneration that presents with gross cortical brain atrophy and altered WM integrity [1–3,7] i.e. processes that lead to decreased heterogeneity of the brain tissue. Having said that, we propose DKI parameters as valuable translational diagnostic markers that seem to closely reflect distinct patterns of ongoing brain changes in various cognitive PD subtypes.

We first demonstrated that DKI reflects specific pathological processes in the brain of two different animal models of PD: a TNWT-61 genetic mouse model overexpressing human alpha-synuclein [4], and a toxic methamphetamine-induced PD mouse model [14]. The former model is characterized by alpha-synuclein accumulation in subcortical and cortical brain regions and microglial activation with no brain atrophy [25]; the latter model is characterized particularly by early degeneration of dopaminergic cells [26]. In the first model, we previously detected increased MK in subcortical GM structures and in the motor cortex [4]. These results are in line with the current findings of increased kurtosis of both subcortical and cortical GM in the PD-NC as compared to HC. Immunohistochemical examination of the GM structures of the scanned TNWT-61 mice revealed alpha-synuclein accumulation-induced changes [4]. Moreover, kurtosis parameters were positively correlated with the total alpha-synuclein signal in the thalamus [13]. On the contrary, early losses of dopaminergic cells induced by intraperitoneal administration of methamphetamine induced decreased heterogeneity of the brain tissue that were reflected by a decrease in kurtosis in the SN, striatum, and sensorimotor cortex [14]. This accords well with the current result of decreased M1 kurtosis in the PD-MCI as compared to the PD-NC group.

Using DKI in human PD, Kamagata et al. [6] were the first to show widespread decreases of MK in WM in a small sample of PD compared to HC (10 HC, 12 PD). Surova et al. [10] observed a similar direction of MK changes (decreases) in both WM and the subcortical GM, namely in the putamen. Conversely, Wang et al. [11] reported increased MK of the SN, caudate, putamen, and globus pallidus in the PD group as compared to HC. Of note, the PD subjects were not cognitively tested and therefore, the authors could not compare PD-NC and PD-MCI groups. As mentioned above, our patterns of kurtosis changes within cortical and subcortical ROIs in PD-NC and PD-MCI accord well with the DKI results in animal models of PD although results in mice models of PD and in humans cannot be directly compared. Our findings at least partially shed light on the inconsistencies of previous studies' results in PD patients.

In the PD-NC group, as compared to the HC group, we demonstrated significant increases of kurtosis parameters in the SN as well as in premotor and motor cortices, i.e. areas engaged within the motor basal ganglia-thalamo-cortical loop. Lewy body pathology in the SN that is prominent already at Braak stages III [27], or neural sprouting [24] may all play roles as potential causes of increased hindrance to water diffusion in the GM tissue. On the other hand, the motor cortex is not affected by Lewy body pathology until stage VI [27]. Nevertheless, early cellular alterations with alpha-synuclein aggregation without the formation of Lewy bodies [28] and increased neuronal spine turnover within M1 pyramidal neurons [29] may lead to increased heterogeneity of the tissue and account for kurtosis increases.

In PD-MCI, kurtosis values of the SN were between those in PD-NC and HC and did not significantly differ from either of the groups. In

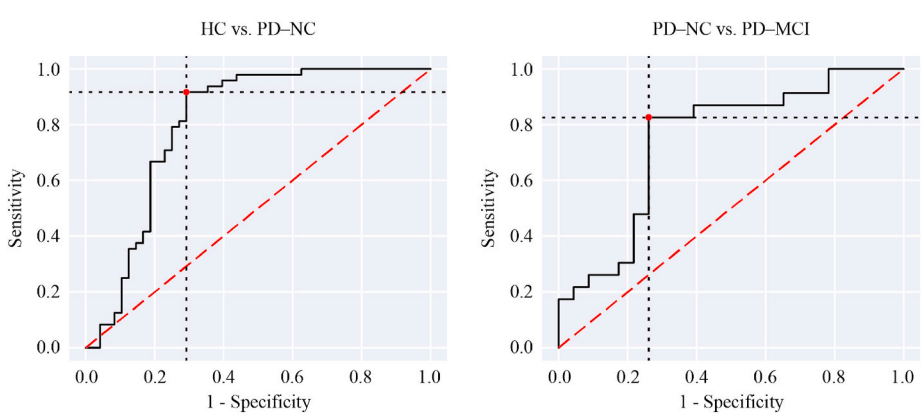

Fig. 3. Differential analysis results, ROC curves.

M1, the PD-MCI group showed significant decrease of kurtosis parameters as compared to PD-NC but they did not differ from the kurtosis values of HC. Similar results were detected also for PMC, thalamus and hippocampus with medium to large ES. These results may reflect an initial neurodegeneration of these areas in MCI patients that co-occurs with the abovementioned cellular changes, such that the positive and negative kurtosis deflection of each balances the other, resulting in kurtosis having almost "normal" values, comparable to those of HC. We cannot exclude other potential explanations for the findings such as an under-detection of kurtosis changes in PD-MCI in the present study, but this seems less probable.

Whereas no significant changes in WM were detected in the PD-NC group, the cognitively altered PD phenotype showed prominent changes in WM as compared to PD-NC and to HC. Changes in the PD-MCI group are not surprising as they suggest altered WM integrity in a more malignant disease subtype. Previous studies also described DTI changes of WM in PD-MCI as compared to HC and/or to PD-NC pointing to decreased WM integrity in the anterior and superior corona radiata, genu, and body of the corpus callosum, anterior and inferior fronto-occipital fasciculus, uncinated fasciculus, and superior and inferior longitudinal fasciculi [30,31]. Note that DBM revealed GM atrophy in frontal regions of PD-MCI only when compared to HC while no significant results were obtained from the PD-MCI and PD-NC comparison. Of note, some authors found WM changes already in early stages of PD [7] and subcortical atrophy in PD as compared to HC using the DBM [22]. Unlike in most of previous studies in the current work we thoroughly examined our groups using a comprehensive cognitive test battery which is our study strength. Nevertheless, we cannot exclude a possibility that the results are specific patient groups-driven and cannot be fully generalized.

All in all, our results reflect deterioration of GM and WM microstructure in different PD phenotypes with and without MCI. Of note, only DKI but not DTI metrics showed significant differences in GM across groups. In PD-NC, increased kurtosis in GM structures including the premotor and motor cortices reflects increased hindrance to water diffusion probably due to early alpha-synuclein-induced microstructural changes. Our PD-MCI group was characterized by profound changes in WM microstructure and gross cortical atrophy. The differential analysis of combined DKI/DTI measures of our GM ROIs showed reasonable accuracy for identifying both PD-NC and PD-MCI subjects.

4.1. Study limitations

The microstructural mechanisms underlying the changes in DKI parameters are discussed in the light of pathological studies in animal models. The human clinico-pathologic studies are needed to further determine neural underpinnings of the DKI changes in the human PD brain. Motivated by our animal studies we focused on the motor basal ganglia-thalamo-cortical loop, including the PMC and M1 cortical regions. Future studies should explore the whole cerebral cortex using the DKI. The study participants were recruited as consecutive cases and we were not successful in perfect matching of all three groups for age and gender. Despite the fact that all analyses were controlled for age, gender, years of education (and LED in the PD groups) we cannot fully exclude a possible effect of unequally distributed participants in respective groups. Since we compared the PD groups with HC only, we cannot conclude on the specificity of our PD-MCI results and further research should focus on comparing MCI groups with various brain pathologies. In the differential analysis, we used a classical cross-validation scheme during the hyper-parameters search. The use of nested cross-validation would be more appropriate for studies with larger datasets.

Disclaimer

The article reflects only the author's view and the Research Executive Agency (REA) is not responsible for any use that may be made of the information it contains.

Financial disclosures

The authors have nothing to disclose.

Acknowledgement

The work was supported by EU Joint Programming initiative within Neurodegenerative Diseases, funded by the Norwegian Strategic Research Council (JPND, APGeM—Preclinical genotype-phenotype predictors of Alzheimer's disease and other dementias, Grant Agreement Number 3056–00001) and by the European Union's Horizon 2020 research and innovation programme under the Marie Skłodowska-Curie grant agreement No. 734718 (CoBeN). We acknowledge the Multimodal and Functional Imaging Laboratory supported by the Czech-BioImaging large RI project (LM2018129 funded by MEYS Czech Republic) and the European Regional Development Fund-Project „National infrastructure for biological and medical imaging" (No. CZ.02.1.01/0.0/0.0/16_013/0001775) for support with obtaining scientific data presented in this paper. This publication was written with the support of the Specific University Research provided by MEYS Czech Republic. We thank Anne Johnson for English language editing. We thank Zuzana Balazova, MD, Lubos Brabenec, Ph.D., Sylvie Kropacova, Ph.D., Kristina Mitterova and Patrik Simko for cognitive data acquisition, and Lubomir Vojtisek, Ph.D., Nikoletta Szabo, MD, Ph.D. and Marek Barton, Ph.D. for consultations regarding the MR data acquisition and processing.

Appendix A. Supplementary data

Supplementary data related to this article can be found at https://doi.org/10.1016/j.parkreldis.2020.10.032.

References

[1] D. Aarsland, B. Creese, M. Politis, K.R. Chaudhuri, D.H. Ffytche, D. Weintraub, C. Ballard, Cognitive decline in Parkinson disease, Nat. Rev. Neurol. 13 (2017) 217–231, https://doi.org/10.1038/nrneurol.2017.27.
[2] L. Krajcovicova, P. Klobusiakova, I. Rektorova, Gray matter changes in Parkinson's and Alzheimer's disease and relation to cognition, Curr. Neurol. Neurosci. Rep. 19 (2019), https://doi.org/10.1007/s11910-019-1006-z.
[3] H. Braak, J.R. Bohl, C.M. Müller, U. Rüb, R.A.I. de Vos, K. Del Tredici, Stanley, Fahn lecture 2005: the staging procedure for the inclusion body pathology associated with sporadic Parkinson's disease reconsidered, Mov. Disord. 21 (2006) 2042–2051, https://doi.org/10.1002/mds.21065.
[4] A. Khairnar, J. Ruda-Kucerova, N. Szabó, E. Drazanova, A. Arab, B. Hutter-Paier, J. Neddens, P. Latta, Z. Starcuk, I. Rektorova, Early and progressive microstructural brain changes in mice overexpressing human α-synuclein detected by diffusion kurtosis imaging, Brain Behav. Immun. 61 (2017) 197–208, https://doi.org/10.1016/j.bbi.2016.11.027.
[5] K.I. Taylor, F. Sambataro, F. Boess, A. Bertolino, J. Dukart, Progressive Decline in Gray and White Matter Integrity in de novo Parkinson's Disease: an Analysis of Longitudinal Parkinson Progression Markers Initiative Diffusion Tensor Imaging Data, Front. Aging Neurosci. 10 (2018) 1–9, https://doi.org/10.3389/fnagi.2018.00318.
[6] K. Kamagata, H. Tomiyama, T. Hatano, Y. Motoi, O. Abe, K. Shimoji, K. Kamiya, M. Suzuki, M. Hori, M. Yoshida, N. Hattori, S. Aoki, A preliminary diffusional kurtosis imaging study of Parkinson disease: comparison with conventional diffusion tensor imaging, Neuroradiology 56 (2014) 251–258, https://doi.org/10.1007/s00234-014-1327-1.
[7] C. Atkinson-Clement, S. Pinto, A. Eusebio, O. Coulon, Diffusion tensor imaging in Parkinson's disease: review and meta-analysis, NeuroImage Clin 16 (2017) 98–110, https://doi.org/10.1016/j.nicl.2017.07.011.
[8] J.H. Jensen, J.A. Helpern, MRI quantification of non-Gaussian water diffusion by kurtosis analysis, NMR Biomed. 23 (2010) 698–710, https://doi.org/10.1002/nbm.1518.
[9] C. Andica, K. Kamagata, T. Hatano, Y. Saito, K. Ogaki, N. Hattori, S. Aoki, MR biomarkers of degenerative brain disorders derived from diffusion imaging, J. Magn. Reson. Imag. (2019) 1–17, https://doi.org/10.1002/jmri.27019.
[10] Y. Surova, B. Lampinen, M. Nilsson, J. Lätt, S. Hall, H. Widner, Swedish BIOFIDER study, D. van Westen, O. Hansson, Alterations of Diffusion Kurtosis and Neurite Density Measures in Deep Grey Matter and White Matter in Parkinson ' S Disease, PloS One (2016) 1–19, https://doi.org/10.1371/journal.pone.0157755.
[11] J.J. Wang, W.Y. Lin, C.S. Lu, Y.H. Weng, S.H. Ng, C.H. Wang, H.L. Liu, R.H. Hsieh, Y.L. Wan, Y.Y. Wai, Parkinson disease: diagnostic utility of diffusion kurtosis

imaging, Radiology 261 (2011) 210–217, https://doi.org/10.1148/radiol.11102277.
[12] V.R. Mishra, K.R. Sreenivasan, X. Zhuang, Z. Yang, D. Cordes, R.R. Walsh, Influence of analytic techniques on comparing DTI-derived measurements in early stage Parkinson's disease, Heliyon 5 (2019), https://doi.org/10.1016/j.heliyon.2019.e01481.
[13] A. Khairnar, J. Ruda-Kucerova, E. Drazanova, N. Szabó, P. Latta, A. Arab, B. Hutter-Paier, D. Havas, M. Windisch, A. Sulcova, Z. Starcuk, A. Király, I. Rektorova, Late-stage α-synuclein accumulation in TNWT-61 mouse model of Parkinson's disease detected by diffusion kurtosis imaging, J. Neurochem. 136 (2016) 1259–1269, https://doi.org/10.1111/jnc.13500.
[14] A. Arab, J. Ruda-Kucerova, A. Minsterova, E. Drazanova, N. Szabó, Z. Starcuk, I. Rektorova, A. Khairnar, Diffusion kurtosis imaging detects microstructural changes in a methamphetamine-induced mouse model of Parkinson's disease, Neurotox. Res. 36 (2019) 724–735, https://doi.org/10.1007/s12640-019-00068-0.
[15] G.E. Alexander, M.R. DeLong, P.L. Strick, Parallel organization of functionally linking basal ganglia and cortex, Annu. Rev. Neurosci. 9 (1986) 357–381, https://doi.org/10.1146/annurev.ne.09.030186.002041.
[16] I. Litvan, J.G. Goldman, A.I. Tröster, B.A. Schmand, D. Weintraub, R.C. Petersen, B. Mollenhauer, C.H. Adler, K. Marder, C.H. Williams-Gray, D. Aarsland, J. Kulisevsky, M.C. Rodriguez-Oroz, D.J. Burn, R.A. Barker, M. Emre, Diagnostic criteria for mild cognitive impairment in Parkinson's disease: movement Disorder Society Task Force guidelines, Mov. Disord. 27 (2012) 349–356, https://doi.org/10.1002/mds.24893.
[17] P. Klobusiakova, R. Marecek, J. Fousek, E. Vytvarova, I. Rektorova, Connectivity between brain networks dynamically reflects cognitive status of Parkinson's disease: a longitudinal study, J. Alzheimers Dis. 67 (2019) 971–984, https://doi.org/10.3233/JAD-180834.
[18] N. Nemcova Elfmarkova, M. Gajdos, I. Rektorova, R. Marecek, S.Z. Rapcsak, Neural evidence for defective top-down control of visual processing in Parkinson's and Alzheimer's disease, Neuropsychologia 106 (2017) 236–244, https://doi.org/10.1016/j.neuropsychologia.2017.09.034.
[19] L. Anderkova, M. Barton, I. Rektorova, Striato-cortical connections in Parkinson's and Alzheimer's diseases: relation to cognition, Mov. Disord. 32 (2017) 917–922, https://doi.org/10.1002/mds.26956.
[20] R.B. Postuma, D. Berg, M. Stern, W. Poewe, C.W. Olanow, W. Oertel, J. Obeso, K. Marek, I. Litvan, A.E. Lang, G. Halliday, C.G. Goetz, T. Gasser, B. Dubois, P. Chan, B.R. Bloem, C.H. Adler, G. Deuschel, MDS clinical diagnostic criteria for Parkinson's disease, Mov. Disord. 30 (2015), https://doi.org/10.1002/mds.26424.
[21] S.M. Smith, M. Jenkinson, H. Johansen-Berg, D. Rueckert, T.E. Nichols, C. E. Mackay, K.E. Watkins, O. Ciccarelli, M.Z. Cader, P.M. Matthews, T.E.J. Behrens, Tract-based spatial statistics: voxelwise analysis of multi-subjects diffusion data, Neuroimage 31 (2006) 1487–1505, https://doi.org/10.1016/j.neuroimage.2006.02.024.
[22] Y. Zeighami, M. Ulla, Y. Iturria-Medina, M. Dadar, Y. Zhang, K.M.-H. Larcher, V. Fonov, A.C. Evans, D.L. Collins, A. Dagher, Network structure of brain atrophy in de novo Parkinson's disease, Elife 4 (2015) 1–20, https://doi.org/10.7554/eLife.08440.
[23] P.L. McGeer, E.G. McGeer, Inflammation and neurodegeneration in Parkinson's disease, Park. Relat. Disord. 10 (2004), https://doi.org/10.1016/j.parkreldis.2004.01.005. S3–S7.
[24] M.H.G. Monje, J. Blesa, M.Á. García-Cabezas, J.A. Obeso, C. Cavada, Changes in thalamic dopamine innervation in a progressive Parkinson's disease model in monkeys, Mov. Disord. 35 (2020) 419–430, https://doi.org/10.1002/mds.27921.
[25] M.-F. Chesselet, F. Richter, C. Zhu, I. Magen, M.B. Watson, S.R. Subramaniam, A progressive mouse model of Parkinson's disease: the thy1-aSyn ("Line 61") mice, Neurotherapeutics 9 (2012) 297–314, https://doi.org/10.1007/s13311-012-0104-2.
[26] P.K. Sonsalla, N.D. Jochnowitz, G.D. Zeevalk, J.A. Oostveen, E.D. Hall, Treatment of mice with methamphetamine produces cell loss in the substantia nigra, Brain Res. 738 (1996) 172–175, https://doi.org/10.1016/0006-8993(96)00995-x.
[27] H. Braak, E. Ghebremedhin, U. Rüb, H. Bratzke, K. Del Tredici, Stages in the development of Parkinson's disease-related pathology, Cell Tissue Res. (2004) 121–134, https://doi.org/10.1007/s00441-004-0956-9.
[28] J.N. Caviness, L. Lue, T.G. Beach, J.G. Hentz, C.H. Adler, L. Sue, R. Sadeghi, E. Driver-Dunckley, V.G. Evidente, M.N. Sabbagh, H.A. Shill, D. Walker, Parkinson's disease, cortical dysfunction, and alpha-synuclein, Mov. Disord. 26 (2011) 1436–1442, https://doi.org/10.1002/mds.23697.
[29] L. Guo, H. Xiong, J.-I. Kim, Y.-W. Wu, R.R. Lalchandani, Y. Cui, Y. Shu, T. Xu, J. B. Ding, Dynamic rewiring of neural circuits in the motor cortex in mouse models of Parkinson's disease, Nat. Neurosci. 18 (2016) 1299–1309, https://doi.org/10.1038/nn.4082.
[30] F. Agosta, E. Canu, E. Stefanova, L. Sarro, A. Tomić, V. Špica, G. Comi, V.S. Kostić, M. Filippi, Mild cognitive impairment in Parkinson's disease is associated with a distributed pattern of brain white matter damage, Hum. Brain Mapp. 35 (2014) 1921–1929, https://doi.org/10.1002/hbm.22302.
[31] T.R. Melzer, R. Watts, M.R. MacAskill, T.L. Pitcher, L. Livingston, R.J. Keenan, J. C. Dalrymple-Alford, T.J. Anderson, White matter microstructure deteriorates across cognitive stages in Parkinson disease, Neurology 80 (2013) 1841–1849, https://doi.org/10.1212/WNL.0b013e3182929f62.